Examination of uncertainty in per unit area estimates of aboveground biomass using terrestrial lidar and ground data.

Michael Shettles [1], Thomas Hilker [2,3*] and Hailemariam Temesgen [2]

[1] U.S. Forest Service, 2150 Centre Ave, Bldg A, Suite 341a; E-Mails: michaelashettles@fs.fed.us

[2] Oregon State University, 204 Peavy Hall, Corvallis, OR; E-Mails: Thomas.hilker@oregonstate.edu, hailemariam.temesgen@oregonstate.edu

[3] University of Southampton, Department of Geography and Environment, Highfield Rd, Southampton SO17 1BJ, United Kingdom

* Author to whom correspondence should be addressed; E-Mail: T.Hilker@soton.ac.uk; Tel.: +1-542-737-2608; Fax: +1-541-737-8410.

Abstract: In estimating aboveground forest biomass (AGB), three sources of error that interact and propagate include: (1) measurement error, the quality of the tree-level measurement data used as inputs for the individual-tree equations; (2) model error, the uncertainty about the equations of the individual trees; and (3) sampling error, the uncertainty due to having obtained a probabilistic or purposive sample, rather than a census, of the trees on a given area of forest land. Monte Carlo simulations were used to examine measurement, model and sampling error, and to compare total uncertainty between models, and between a phase-based terrestrial laser scanner (TLS) and traditional forest inventory instruments. Input variables for the equations were diameter at breast height, total tree height (defined the height from the uphill side of the tree to the tree top) and height to crown base; these were extracted from the terrestrial LiDAR data.

Relative contributions for measurement, model and sampling error were 5%, 70% and 25%, respectively when using TLS, and 11%, 66% and 23%, respectively when using the traditional inventory measurements as inputs into the models. We conclude that the use of TLS can reduce measurement errors of AGB compared to traditional measurement approaches.

Keywords: Model error; sampling error; measurement error; Pacific Northwest

1. Introduction

Forest inventory and monitoring programs such as the United States Department of Agriculture (USDA) Forest Inventory and Analysis Program (FIA) produce estimates and reports of forest resources that bear increasing utility for agencies and other users alike. Inventory attributes derived from such estimates often lack a defensible magnitude of certainty to support forest management decisions that satisfy an array of ecological, economic and social requirements. An accurate depiction of the precision of such estimates would serve to guide and support such decisions. With the growing use of FIA inventory data for attributes such as aboveground biomass (AGB), gains in precision made by addressing specific sources of uncertainty could benefit forest managers and planners, as well as scientists drawing inference and making decisions from their AGB estimates (Temesgen et al. 2015).

The reliability of AGB estimates produced using sampling approaches such as FIA depends on three primary sources of uncertainty that interact and propagate: (1) the quality of the tree-level measurements used as inputs for estimating biomass of individual trees; (2) the uncertainty about the models used for predictions; and (3) the uncertainty due to having obtained a probabilistic sample, rather than a census, of the trees on a given area of forest land (Cunia 1965). Increasing emphasis on acquiring highly accurate estimates of AGB for management and policy decision making also requires transparent characterizations of associated uncertainty stemming from the three sources of error mentioned above. Accurate estimation of these uncertainties requires accounting for all three of the aforementioned sources of uncertainty when constructing reliability statements for AGB. However, many forest inventory operations currently only account for sampling uncertainties, as the first two uncertainties listed are more difficult to estimate from field-based measures alone, and are often assumed to be of less importance. Besides allowing more confidence in landscape level predictions, estimation of all three sources of uncertainty may also provide an opportunity to observe possible gains in precision to be had by addressing uncertainty that arises due to issues with tree-level explanatory measurement data. These have practical implications for instance in terms of the choice of instrument, calibration and standardized training and implementation procedures for data collection (Weiskittel et al. 2011, p.277 and Temesgen et al. 2007).

Difficulties in estimating accuracy of tree-level measurements include the collection of suitable ground truth data to base uncertainty estimates on. Henning and Radtke (2006) compared diameter outside bark (DOB) measurements of nine destructively sampled loblolly pine (*Pinus taeda*) trees to the same DOB measurements obtained using a terrestrial laser scanner (TLS). DOBs, measured in 1m intervals, were reported to be within 1-2cm, with greater accuracy achieved for stem portions below the base of live crown. Bienert et al. (2006) and Maas et al. (2008) reviewed and compared work flow and data processing procedures for extracting common inventory attributes such as DOBs and total tree height (HT). As an alternative to these destructive methods, TLS may provide new opportunities to provide ground truthing estimates for current inventory approaches, which typically predict tree metrics based upon a few easily acquired measurements, such as diameter at breast height (DBH) and height. TLS may help us to improve upon these estimates by providing high density point clouds, useful for accurately depicting stem properties, including taper, as well as crown metrics, including crown density and leaf area. For instance, TLS has been used for measuring tree-level metrics such as DOBs and bole heights (Simonse et al. 2003, Hopkinson et al. 2004, Henning and Radtke 2006, Bienert et al. 2006, Maas et al. 2008, Weiß 2009, Pueschel et al. 2013, Liang et al. 2014) as well as crown metrics such as height to crown base and crown volume (Chasmer at al. 2006, Jung et al. 2011).

Hauglin et al., (2013) determined the biomass of Norway spruce with TLS using voxel-based approaches and crown dimension features. Other techniques include stem reconstruction (Yu et al., 2013), as well as total tree reconstruction (Calders et al., 2014 and Hackenberg et al., 2014). The performance of TLS in obtaining specific individual-tree variables has been demonstrated, including taper (Thies et al. 2004), DOB (Simonse et al. 2003, Hopkinson et al. 2004, Henning and Radtke 2006, Bienert et al. 2006, Maas et al. 2008, Weiß 2009, Pueschel et al. 2013), canopy metrics such as crown area, crown volume and height to crown base (HTCB) (Chasmer at al. 2006, Jung et al. 2011), and bole reconstruction for stem volume calculation (Yu et al. 2013). Chasmer et al. (2006) used coinciding ALS and TLS data to compare against field-based plot measurements of HT, HTCB and maximum crown width. Average height estimate biases were similar for both ALS and TLS at 1.1m and 1.2m, respectively. ALS overestimated HTCB by an average of 1.4m due to point density distributions being weighted toward the top of the tree, whereas TLS underestimated HTCB by 6.4m, not only resulting from the inverse of the aforementioned distribution due to an inverted perspective, but largely due to not accounting for the occurrence of dead branches.

Unique to this study is the depiction of how the measurement performance of TLS in extracting these tree-level variables translates into differences in per unit area estimates of forest-related parameters, specifically AGB. We investigate how the total propagated error of AGB associated with using a TLS compares to that associated with using common forest inventory instruments used for standing tree measurements. To do so, we used data from three types of measurements performed on 25 lodgepole pine (*Pinus contorta* Douglas) trees as the basis for making these comparisons. We validate the estimates obtained from TLS and traditional forest inventory instruments against estimates obtained by destructive sampling methods. Using a newly developed set of Component Ratio Method (CRM) equations for predicting lodgepole pine AGB, a Monte Carlo simulation approach was employed for making comparisons between associated uncertainties of per unit area estimates of AGB for each measurement method.

2. Methods

2.1. Study locations

In order to capture some regional differences in tree form, the data for this study were collected from both the Willamette National Forest (WNF) and the Deschutes National Forest (DNF) in western and central Oregon, USA, respectively. All locations were within an intermediate-elevation range, with the WNF locations spanning from 1,160-1,340 meters above sea level and the DNF locations from 1,280 to 1,340 meters. The WNF locations encompassed two forest types: (1) a diverse mixed-species coniferous forest, with observed species being Douglas-fir (*Pseudotsuga menziesii* var. menziesii), western hemlock (*Tsuga heterophylla* (Raf.) Sarg.), lodgepole pine, mountain hemlock (*Tsuga mertensia*na (Bong.) Carr.), noble fir (*Abies procera* Rehder), Engelmann spruce (*Picea engelmannii* Parry ex Engelm.), and western white pine (*Pinus monticola* Douglas ex D. Don); and (2) a homogenous coniferous forest composed of primarily lodgepole pine and with a small element of grand fir (*Abies grandis* (Douglas ex D. Don) Lindley). The DNF locations also included one forest type of homogenous coniferous species composition, with observed species being lodgepole pine and ponderosa pine (*Pinus ponderosa* Douglas ex C.Lawson).

2.2. Field measurement approach

Trees were selected via subjectively and common forest inventory variables including DBH, HT and crown ratio (CR) were recorded. While the requirement for accessibility for felling limited our ability to select trees randomly, efforts were taken to select sample trees either located in different forest stands, or sufficiently distanced apart to avoid issues of spatial autocorrelation. A total of 25 trees were destructively measured over a four week period during July and August 2013. DBH, HT and CR ranged from 13.5 to 42.9 cm, 9.2 to 31.9 m and 0.30 to 0.948, respectively. Standing-tree measurements (STM) were conducted prior to felling, with DBH being measured using a Spencer combination tape and with both HT and HTCB being measured using a Trupulse Laser Rangefinder 360R. For this study, HTCB was defined as the bole height of the first live limb (i.e., the lowest branch with green needles on it). Among the measurements taken to obtain reference values of AGB, downed-tree estimates of HT and HTCB were measured with an open reel fiberglass tape.

For estimation of component biomass per unit area, ground plot data were collected from those forest stands from which the 25 sample trees were sourced. This ground plot data consisted of 25 cluster plots, each comprised of four circular fixed area subplots arranged around each sample tree. A 0.017 hectare plot was the primary subplot (radius 7.33 m), with the pith of the sample tree as the center. The centers of the other three circular subplots were located 36.58 m at azimuths of 120, 240 and 360° from the pith of the sample tree. The area of these other three subplots was 0.008 hectares (radius 5.18 m). Within each subplot, all trees (> 10.16 cm diameter) were measured and/or recorded for attributes such as species, DBH, HT and HTCB, among others.

2.3. TLS Field Scanning Protocol

In addition to the standing tree measurements, sample trees were scanned with a tripod-mounted FARO Focus^{3D} 120 TLS prior to felling. As opposed to the more common time-of-flight TLS technology the FARO scanner uses phase shift technology which uses the shifts of modulated waves of returned infrared light pulses to calculate distances traveled (FARO 2014). Maximum ranges of phase-based scanners are less than those of time-of-flight scanners; however, measurement rates (pulses per second emitted) are usually much higher with greater distance accuracies realized than for time-of-flight scanners. See Table 1 for the technical data of the FARO Focus^{3D} 120.

Each sample tree was scanned from three locations around its periphery at distances ranging from approximately 3-8m away from the tree. Scan positions were placed at 120° apart from each other to maximize the information gathered for characterizing the geometric shape of the tree. For automatic co-registration, four manually placed targets were positioned near the sample tree with a minimum of three targets being visible from each scan position. Target construction consisted of printed checkerboard signs affixed to wooden staked panel boards. Because it was desired to maximize information gathered in this study, minimal amounts of understory vegetation deemed obstructive were manually removed.

Scanning was conducted at a speed of 122,000 pulses per second, resulting in approximately seven minutes duration per scan. With transport and setup time between scan positions taking an average of 2-3 minutes, scanning each tree from all three angles took on average 25-30 minutes.

The scan data were collected in a local coordinate system using the scanner location as the origin. Registration was done automatically using SCENE v4.8 software (FARO 2014) based on printed checkerboard targets placed within each scan image. Quality of registration was reported as average discrepancy in distance between a given pair of reference objects or tension (ranging between 1mm to 8mm). For each registered scan, TLS returns belonging to an individual sample tree were selected visually from the 3D representation of the surrounding forest. This process was done by displaying the registered scan and using the visible scan positions to deduce which was the sample tree (Figures 2 and 3). Prior to scanning, boles of the sample trees were wrapped with very thin striped plastic flagging, intentionally placed well above DBH, that proved visible as a final confirmation the correct tree was to be selected from the registered point cloud. These selected points were then exported for later use in extracting DBH, HT and HTCB using Matlab 2013b (The MathWorks, http://www.mathworks.com, USA).

2.4. Tree Parameter Extraction from Selected Scan Data

TLS based height measurements were normalized to the surface elevation by means of a digital terrain model (DTM) derived from the TLS data. Ground and non-ground returns were separated using a grid based approach to select the lowest return within a 0.3048m × 0.3048m sampling grid placed over the plot area.

2.4.1. Tree Detection

With the ground model complete the next step before obtaining tree parameters was to estimate the center of the sample tree at approximately 1.37m (diameter at breast height) above the ground. This estimated location served as a control point from which all measurement algorithms originated from. Similar to Mass et al. (2008) a thin 5-10cm horizontal slice was selected from the point cloud for stem detection (Figure 2). This horizontal slice often included many points representing branches and foliage at that height. To expedite the estimation process only a subset of the points in the slice was used (Figure 3). A nonlinear least squares circle-fitting procedure, similar to that described by Henning and Radtke (2006), was used for estimating the diameter and XY center of each tree. The means of the XY coordinates of all subset points were used as initial estimates, or starting values, for the nonlinear procedure, provided there were no large outliers in the point cloud (Maisonobe 2007). Restriction of the subset to the XY range of the main bole additionally addresses any outliers associated with branches or foliage. The starting value for the diameter of the sample tree consisted of using the following equation to solve for a diameter for each of the subset points, and then using the mean of all calculated diameters, produced using the following equation (Henning and Radtke 2006):

$$\hat{d}_i = 2 \times \sqrt{(\hat{x}_c - x_i)^2 + (\hat{y}_c - y_i)^2} \qquad (1)$$

where $\hat{d}_i$ is estimated diameter for the ith subset point, the $(\hat{x}_c, \hat{y}_c)$ pair are the means of the (x,y) coordinates for all subset points and the (x_i, y_i) pair are the (x,y) coordinates of the ith subset point. With these three starting values and the following equation as the objective function, the three unknowns were solved for by minimizing the sum of squares for all subset points:

$$F_i = 2 \times \sqrt{(\hat{x}_c - x_i)^2 + (\hat{y}_c - y_i)^2} - \hat{d}_i \qquad (2)$$

where F_i is the value of the objective function for the ith subset point and $\hat{x}_c$, $\hat{y}_c$ and $\hat{d}_i$ are the three unknowns. With the spatial location of the center of the tree and its diameter approximated, subsequent measurements stemmed from this information.

2.4.2. Uphill Side of the Tree and Total Height

To conform to forest inventory practices, all heights up the bole to the tip of the sample trees were measured relative to the ground adjacent to the tree with the highest elevation (Avery and Burkhart 2002, p.144). Thus, it was necessary to identify the uphill-side of the tree and determine the elevation of that side relative to the rest of the point cloud. Using the approximated center and diameter, all DTM cells determined to be spatially adjacent to the base of the sample tree were selected. The selected DTM cell with the highest elevation value was determined to be the uphill-side of the tree. The corresponding elevation value of that cell, heretofore referred to as the reference z-value, was used as the minimum reference height for extracting DBH, HT and HTCB.

A statistical quality control was implemented in order to ensure the reference z-value was not a far outlier representing anomalies such as nearby rocks or protruding tree roots. Whereby, if the coefficient of variation (CV) of the elevation values of all the selected adjacent DTM cells was above a defined percentage, the adjacent cell with the next highest elevation value was chosen from the eight cells that bordered the stem center grid cell. For the purpose of this study a subjectively chosen CV of 60% was used to remove outlier values. HT was then simply calculated as the difference between the highest point in the point cloud and the reference z-value. Stray points above the tip of the tree were not observed to be a problem due to the prior filtering using the SCENE software.

2.4.3. Diameter at Breast Height

While the approximated diameter from the previously-described detection slice at breast height could potentially serve as an estimate of DBH, the height at which the slice was taken was 1.37m above the minimum elevation of the entire point cloud, rather than the uphill side of the tree. On steeply sloping terrain, differences in relative bole heights could be substantial. To avoid this issue, an improved DBH was extracted 1.37m above the reference z-value using the previously described procedure of subsetting followed by the non-linear least squares circle-fitting. However, an additional precision constraint was added to maximize the reliability of the DBH measurement. If the root mean square error (RMSE) of the non-linear least squares procedure was above a defined threshold of 5mm, a recursive “noise reduction” method, similar to Henning and Radtke (2006), was invoked. The main purpose of this procedure was to reduce TLS observations originating from nearby branches or understorey. Henning and Radtke (2006) showed the removal of these outliers greatly improved our estimates of DBH. The filtering process involved continually removing the points whose coordinates produced estimated diameters that were the maximum absolute distance from the mean of all estimated diameters until the standard deviation of the estimated diameters was below the same defined threshold. It was observed that using 5mm for this threshold was sufficient for minimizing the measurement error, while also removing stray points around, and not belonging to, the main bole.

2.4.4. Height to Crown Base

Estimation of HTCB was based on analysis of point intensity and percentiles of return height. Point intensity is a measure of the returned energy of an emitted pulse. While intensity values cannot directly be used as a surrogate to optical measures of surface reflectance (as these uncalibrated measurements depend on environmental conditions, scanner properties and location) LiDAR based intensity measures have been successfully used to distinguish between green foliage and non-photosynthetically active tree elements (Popescu et al. 2007, Pesonen et al. 2008 and Kim et al. 2009), due to the large differences in NIR reflectance of these vegetation components. As a result, we used intensity measures to classify between foliage and woody surfaces for the purpose of estimating HTCB. By plotting intensity versus height, an empirical threshold could be determined, below which the intensity values for points returned from foliage would theoretically occur (Figure 4). The subset of points below this threshold served as a representation of the live crown profiles. We then used different percentile heights within this subset of points for different age classes of the trees. Specifically, the 5th, 10th and 25th percentile height of this subset were used to measure HTCB for the 20-40yr, 40-80yr and >80yr age classes of sample trees selected, respectively.

2.5. Modeling biomass

The biomass equations used for this study predict the proportion of AGB for the bole, bark, branch and foliage component (Poudel and Temesgen 2016 and Poudel et al. 2015). These proportions can then be multiplied by an estimate of total tree AGB to obtain the AGB of each tree component. Both the component equations and the total tree biomass equation were fit in separate systems of equations using the seemingly unrelated regression method (SUR) in SAS statistical software (SAS Institute Inc., v9.4). The four CRM component equations and the total tree equation used in our study are of the form (Poudel and Temesgen 2016 and Poudel et al. 2015):

$$\widehat{pBole}_i = \exp[\hat{\beta}_0 + \hat{\beta}_1 \times \ln(DBH_i) + \hat{\beta}_2 \times \ln(HT_I) + \frac{\hat{\sigma}^2_1}{2}] \quad (3)$$

$$\widehat{pBark}_i = \exp[\hat{\beta}_3 + \hat{\beta}_4 \times \ln(DBH_i) + \frac{\hat{\beta}_5}{\ln(HTCB_i)} + \frac{\hat{\sigma}_2^{\,2}}{2}] \quad (4)$$

$$\widehat{pBranch}_i = \exp[\hat{\beta}_6 + \hat{\beta}_7 \times \ln(DBH_i) + \hat{\beta}_8 \times \ln(HTCB_i) + \frac{\hat{\sigma}^2_3}{2}] \quad (5)$$

$$\widehat{pFoliage}_i = \exp[\hat{\beta}_9 + \hat{\beta}_{10} \times \ln(DBH_i) - \hat{\beta}_{11} \times \ln(HTCB_i) + \frac{\hat{\sigma}^2_4}{2}] \quad (6)$$

$$\widehat{Total\ Tree}_i = \exp[\hat{\beta}_{12} + \frac{\hat{\beta}_{13}}{DBH_i} + \frac{\hat{\sigma}_5^{\,2}}{2}] \quad (7)$$

where $\widehat{pBole}_i$, $\widehat{pBark}_i$, $\widehat{pBranch}_i$ and $\widehat{pFoliage}_i$ are the estimated proportions of component AGB for bole wood, bark, branches and foliage, respectively, exp(.) is the exponential function, ln(.) is the natural logarithm function and the $\hat{\beta}s$ are the estimated parameters from the SUR procedure. The $\frac{\hat{\sigma}^2}{2}$ is the correction factor for the resulting bias when back-transforming model predictions from the logarithmic to the initial scale of interest, where $\hat{\sigma}^2$ is the estimated mean squared error, or residual variance (Baskerville, 1972, McRoberts and Westfall 2014).

2.6. Measurement Error Variability

For DBH, HT and HTCB, the differences between the measured values and the downed-tree measurements were calculated for both the TLS and traditional forest inventory instruments. In this study, the downed-tree measurements were considered to be the known “true” values due to the ease with which measurements could be taken as accurately as possible. The summary data for these differences were subsequently calculated for each input variable for the models (Table 2).

It is known that standard deviation of the measurement error is zero when HT is zero. Hence, to stay consistent with the methodologies of Berger et al. (2014) and Shettles et al. (2015)a simple linear regression model through the origin was constructed to predict the standard deviation of the measurement errors. In order to conduct regressions of standard deviation of measurement errors on input variables, HT values were sorted in ascending order and grouped into groups of size 3, with the last group including the remainder of the HT values. With an aim to maximize the number of possible groups, the group size of 3 was symptomatic of a sample size of 25 trees. For every g^{th} group, the means of the HT values and $SD_{ME,g}$ were estimated, where $SD_{ME,g} = \frac{1}{n-1}\sqrt{\sum_{i=1}^{n}\left(ME_{HT,g} - \overline{ME_{HT,g}}\right)^2}$ is the standard deviation of the measurement errors for HT and $ME_{HT,g} = HT_D\ HT_S$ are the HT measurement errors, where HT_D is the downed-tree height measurement, n is the group size and HT_S is the standing-tree height measurement. The following model form was fit to the grouped data for HT using the method of ordinary least squares:

$$\widehat{SD}_{ME,HT} = \hat{\beta}_{14} \times HT \tag{8}$$

where $\widehat{SD}_{ME,HT}$ is the estimated standard deviation of the measurement errors for *HT* and $\hat{\beta}_{14}$ is the model parameter estimate.

2.7. Integrating Simulated Measurement Errors into Model Uncertainty

Using the standard deviations from Table 2 and equation 8, Monte Carlo simulations (>5000 iterations), were used to approximate model uncertainties reflective of the additional uncertainty due to measurement error (Berger et al. 2014). Input variable contamination was implemented as a two part process: First, for the kth component model, a multiplicative factor ~N(1, SD_{HT}^2) was randomly generated and multiplied together with the input variables, where SD_{HT} is the standard deviation of the height measurement errors; and second, an additive factor ~N(0, $\widehat{SD}_{ME,HT}^2$) was randomly generated and added to the input variables, where $\widehat{SD}_{ME,HT}$ is the predicted standard deviation from equation 8 (Berger et al. 2014).

The impact of the additional uncertainty was assessed by calculating the mean prediction and RMSE and the relative RMSE (RRMSE) over all iterations with the following formulas:

$$\text{mean} = \frac{1}{n}\sum_{i=1}^{n} \hat{Y}_i \tag{9}$$

$$\mathrm{RMSE} = \sqrt{\frac{1}{n}\sum_{i=1}^{n}\left(Y_i - \hat{Y}_i\right)^2} \tag{10}$$

where Y_i is the observed value and $\hat{Y}_i$ is the fit for the ith tree. RRMSE is calculated by simply dividing RMSE by the mean.

To convert the predicted proportions and RMSEs to tree-level units (oven-dry kg), the predicted proportions were multiplied by the fitted value for total tree biomass to obtain tree-level fitted values of component AGB (Eq. 7), and multiplied with the absolute RMSEs produced as the square root of the sum of the squared relative RMSEs:

$$\delta AGB_{Comp} = \widehat{AGB}_{Comp} \times \sqrt{\left(\frac{\delta AGB_{Ratio}}{\widehat{AGB}_{Ratio}}\right)^2 + \left(\frac{\delta AGB_{TT}}{\widehat{AGB}_{TT}}\right)^2} \tag{11}$$

Where δAGB_{Comp} is the combined RMSE in tree-level units, δAGB_{Ratio} is the RMSE for the CRM component ratios and δAGB_{TT} is the RMSE for Total Tree AGB (equation 7).

2.8. Integrating Model Error into Sampling Uncertainty

In order to integrate the model errors into the sampling uncertainty, the magnitude of the model errors integrated needed to be contingent upon the magnitude of the model predictions. Using the previously described grouping approach with respect to the model errors, a simple linear regression model (also forced through the origin) was constructed to predict the magnitude of the model errors. Following the notation and general methodology of McRoberts and Westfall (2014): (1) for the kth component model, a joined list of ε_i, Y_i and $\hat{Y}_i$ was created and sorted in ascending order with respect to $\hat{Y}_i$, where $\varepsilon_i = \hat{Y}_i - Y_i$; (2) the sorted triads of observations were grouped into groups of size 3, with the last group including the remainder of the observations; (3) for every gth group, the mean observation $\bar{Y}_g = \frac{1}{n_g}\sum_{i=1}^{n_g} Y_i$, the mean fitted value $\bar{\hat{Y}}_g = \frac{1}{n_g}\sum_{i=1}^{n_g} \hat{Y}_i$ and the mean square error $\sigma_g{}^2 = \frac{1}{n_g-1}\sum_{i=1}^{n_g} \varepsilon_i{}^2$ were calculated, where n_g is the number of trees in the gth group; (4) the following model form was fit to the grouped data for each component model using the method of ordinary least squares

$$\hat{\sigma}_i = \hat{\beta}_{15} * \hat{Y}_i \tag{12}$$

Where $\hat{\sigma}_i$ is the predicted model error for the ith tree, $\hat{\beta}_{15}$ is the model parameter estimate and $\hat{Y}_i$ is the model fitted value for the ith tree. It should be noted that with measurement error integrated into the model errors, the value of $\hat{\beta}_{15}$ is expected to increase, reflecting this additionally accounted for source of uncertainty.

A bootstrapping technique, in conjunction with equation 12, was used to simulate the effects of model errors on the uncertainty of per unit area estimates of component AGB for all models. A similar Monte Carlo simulation sequence and notation described by McRoberts and Westfall (2014) was used for each component model.

First, the data set containing the "true" values of the 25 sample trees was randomly sampled with replacement to produce a bootstrapped-sample of size 25. Similar to the previously described method of simulating measurement errors, contaminated model predictions for all 25 bootstrapped-sampled trees were produced by adding a randomly generated residual, $\varepsilon_i \sim N(0, \hat{\sigma}_i^2)$, to the prediction for the ith pseudo-sampled tree produced using the kth component model, where $\hat{\sigma}_i$ is estimated using equation 12. Using the contaminated predictions and the pseudo sample data, a new model, of the same form as the kth component model, was refit. For equations 3, 4, 5, 6 and 7, due to their original model form, the contaminated predictions and the pseudo sample data required transformation to the $\log_{10}$-$\log_{10}$ and ln-ln scale, respectively, prior to refitting.

Second, the refit equations were applied to the ground plot data set. For the ith tree in the jth plot, predictions of tree-level component AGB were produced by adding the model predictions to a randomly generated constrained residual, $\lambda\varepsilon_i$ where ε_i is the randomly generated residual ~N(0, $\hat{\sigma}_i^2$), and λ is a multiplicative constraining factor that yields model efficiency values of 0.95. Model efficiency, calculated as

$$Q^2 = 1 - \left(\frac{\sum_{i-1}^{n_{pl}} e_i^{\,2}}{\sum_{i=1}^{n_{pl}} (Y_i - \bar{Y})^2} \right) \tag{13}$$

where n_{pl} is the number of trees in the ground plot data set, is a goodness-of-fit statistics similar to the coefficient of determination from the ordinary least squares procedure, where the higher the value the better the fit of the model to a given data set (Vanclay and Skovsgaard 1997, McRoberts and Westfall 2014). This multiplicative factor constraint was implemented in order to have a standardized quality of fit of the model to the ground plot data for purposes of comparing the standard errors of the mean for all component models. Due to recent published findings illustrating the minimal effect correlation among trees within plots has on the standard error of the estimates, correlation among residuals was not integrated into the analysis of this study (Berger et al. 2014, Breidenbach et al. 2014, McRoberts et al. 2014).

Third, to obtain the estimated per hectare values of component AGB on the jth cluster plot, the summation of all subplot-level per unit area component AGB predictions on the lth subplot were calculated as

$$Y_j = \sum_{l=1}^{4} Y_l \tag{14}$$

with

$$Y_l = \frac{\sum_{l=1}^{n_l} Y_{i,l}}{Subplot\ Area_{hectares}} \quad (15)$$

Where n_l is the number of trees observed in the lth subplot and $Y_{i,l}$ is the ith tree on the lth subplot. Fourth, for each simulation cycle the mean and variance of the mean across all cluster plots were calculated as

$$\bar{Y} = \frac{1}{n_{cl}} \sum_{j=1}^{n_{cl}} Y_j \quad (16)$$

$$\widehat{\mathrm{Var}}(\bar{\mathrm{Y}}) = \frac{1}{n_{ci}(n_{cl}-1)} \sum_{j=1}^{n_{cl}} \left(Y_j - \bar{Y}\right)^2 \quad (17)$$

Where n_{cl} is the number of cluster plots (25 in this study). Finally, the mean prediction and mean within-simulation variance over 5000 simulation cycles were calculated as

$$\hat{\mu}_{sim} = \frac{1}{5000} \sum_{1}^{5000} \bar{\mathrm{Y}} \quad (18)$$

$$\widehat{\mathrm{Var}}_{sim} = \frac{1}{5000} \sum_{1}^{5000} \widehat{\mathrm{Var}}(\bar{\mathrm{Y}}) \quad (19)$$

Comparisons of the mean predictions as well as final propagated error were compared for all component models for both approaches. Metrics used for comparison included RMSE, RRMSE, standard error of the mean (SE) from equation 19 and relative SE (RSE).

3. Results and Discussion

3.1. Measurement Errors

Table 2 shows the measurement error summary statistics for input variable measurements using the TLS and the STM. The circle-fitting procedure for measuring DBH resulted in 6 of the 25 trees showing agreement with the downed tree measurements, and 9 being within 3cm. These results are comparably better than previous studies assessing the quality of TLS-derived diameter measurements. Simonse et al. (2003) used a Hough-transformation to obtain DBH for 23 trees, reporting minimum, maximum, mean and standard deviation of measurement error values as -5.8cm, 5.6cm, 1.7cm and 2.8cm, respectively. Hopkinson et al. (2004) reported an average difference of 10cm for plot-level comparison of DBH between TLS and manual measurement techniques. Thies et al. (2004) used a stem reconstruction method involving the fitting of a series of cylinders up the main stem of two scanned deciduous trees of different species. DBH was calculated as the diameter of the corresponding cylinder at breast height. Deviations in TLS-derived DBH measurements from standing tree measurements were -1.3cm and 0.6cm for European beech and wild cherry, respectively. Henning and Radtke (2006) reported errors of less than 1cm (0.3in) using a similar circle-fitting procedure as the one described here when comparing TLS diameters to known values from felled trees. In a separate study attempting to model 3D plot-level forest structure, Henning and Radtke (2006) reported an average DBH difference of 4.8cm when comparing TLS measurements to standing tree measurements. Most likely, the quality of our TLS-derived DBH results compared to other studies is largely attributable to our multi-scan approach, which has been shown to reduce the variability TLS-derived DBH measurements by drastically increasing the cover of point clouds (Pueschel et al. 2013). Using a multi-scan dataset and quantitative structure models to obtain inferred ABG through estimated total height and DBH, Calders et al, 2014 reported a concordance correlation coefficient of 0.98. A RMSE threshold below 5mm often resulted in underestimations of DBH. Presumably, this was due to points on the outside of the fissures of the bark being the points removed first during this point removal process. Because the true values of DBH were measured on the outside of these fissures, stricter thresholds were not used. Hence, if this procedure is to be used for older trees of a species with deeply fissured bark characteristics, this process may require allowing for higher RMSE thresholds. Average RMSE observed for the fitting of all 25 DBHs was 3.99 mm. This process holds promise for obtaining upper stem diameters outside bark for purposes of taper determination, form factor calculation and possible merchantable height identification as well. While more robust methods exist for stem detection and outlier determination that do not rely on a circularity tolerance, these results are still relevant to assessing uncertainty in AGB estimates obtained through TLS, a topic studied little up to this point.

HT measurement error results for TLS showed lower average bias than the STM HT measurements at -0.1m and -1.0m for TLS and STM, respectively. Encouragingly, the standard deviation of these measurement errors for HT was also lower for TLS, at 0.3m and 0.7m for TLS and STM, respectively. These estimates are lower than those reported by Hopkinson et al. (2004), who reported an average difference of 1.5m for plot-level HT comparisons between TLS and manual measurement techniques. Their reported difference in standard deviations of HT measurements was lower at 0.2m. Chasmer et al (2006) reported an average underestimation of HT of 1.2m for 15 trees within a closed-canopy stand of red pine (*Pinus resinosa*) scanned from five different locations. The comparative improvement upon these studies suggests this method of identifying a reference z-value from which to subtract from the maximum z-value is superior to other methods. However, with stand density and tree size being limiting factors in the accuracy of TLS-derived-HT measurements, the quality of the results we present here for HT could also likely be a result of several of the sample trees being from stands with lower stand densities, and lodgepole pine being a relatively shorter tree species. The capability of the FARO Focus^{3D} 120 to scan at the point density chosen for this study also likely furthered this improvement.

In contrast to HT, HTCB results for the TLS exhibited a larger mean and standard deviation of the measurement errors compared to the STM. However, this variable has typically been a point of imprecision for TLS extraction procedures. Thies et al. (2004) reported differences in HTCB values of -0.12m and -0.11m for the two aforementioned sample trees. With the sample trees being relatively large, forked and deciduous, HTCB was measured as the height to the first fork. Jung et al. (2011) compared HTCB measurements from coincident ALS and TLS data, where the TLS measurements were considered to be the actual values. ALS HTCB values were obtained using k-means clustering technique which groups the point cloud into a user-defined number of classes based upon differences in the spatial distribution of points within the point cloud. The authors chose three classifications to represent ground cover, understory vegetation and canopy cover. ALS HTCB was determined from the lowest point in the canopy cover classification. Because differences in the point density distribution were deemed too small with the TLS data, k-means clustering was not used, replaced by manual identification of the lowest crown return via a monitor display. The difference in mean HTCB values was reported as 0.2m.

Using the height of the lowest point in this subset as a measure of HTCB resulted in consistent underestimation, similar to the results observed by Chasmer et al. (2006). This was likely due to: (1) the presence of dead branches interspersed within the lower portion of the live crown, as is common for lodgepole pine; and (2) the definition of HTCB used in this study being the height to the lowest live limb rather than the height to the lower margin of the main live crown. Thus, HTCB was then estimated as the 5th, 10th and 25th percentile height of this subset for the 20-40yr, 40-80yr and >80yr age classes of sample trees selected, respectively. Selection of this threshold was based upon: (1) empirical observation; and (2) the knowledge that younger lodgepole pine trees typically have lower HTCB values and fewer dead branches. Due to this method yielding the lowest average measurement error, the measurements resulting from this approach were ultimately selected for use in the subsequent error propagation analysis.

Our results show that applying the TLS inventory parameter extraction techniques to inventory applications could be a useful approach to complement conventional data acquisition techniques; however, further validation will be needed for broader scale applications across different forest types/larger areas. We acknowledge that sampling conditions and sample size of 25 destructively measured trees is not sufficiently representative to extrapolate our findings across larger areas or different vegetation types. Our approach should therefore be understood as a first demonstration of error and error propagation obtainable from terrestrial laser scanning using ground data in PNW forests.

Future improvements would further bolster the applicability of TLS to larger operations. First, rather than the manual graphical method for tree detection employed here, more sophisticated automatic tree detection procedures that omit non-bole points from branches and foliage, would be necessary. Secondly, for the subsetted percentile approach for HTCB, the tree size to percentile relationship may need to be more generalized by diameter classes, or calibrated to the specific operation.

3.2. Model Predictions and Uncertainty

When the measurement error was integrated into the CRM equations, mean predictions of AGB for all components were similar between instruments (Table 4). The TLS RMSE values for the CRM ratios were lower for all components compared to the STM RMSE values (Table 5). However, the RMSE values were larger for the TLS, primarily due to the Total Tree SUR equation having a 147% larger RMSE. This can be attributed to the assumption that the STM measurement of DBH, the only input variable for the SUR equation, was measured without error, hence the STM simulation procedure did not involve the contamination of DBH values. Had the measurement error in DBH been assessed, it is feasible to reason that the uncertainty value for the STM SUR equation would have been greater than the 70.59kg value reported in this study. Also worthy of noting, the magnitude of the difference between STM and TLS may have been less dramatic when the total tree equation would have been fit in a common system of equations. Nevertheless, the tree-level uncertainty in predicted component AGB associated with using the TLS for extracting input variables for the CRM equations is likely greater than estimates using a spencer tape by trained individuals.

3.3. Per Unit Area Estimates and Uncertainty

With model errors incorporated into the simulations for per unit area estimation, the uncertainty increased markedly (Tables 6 & 7). This notable increase is further illustrated in Table 9, which shows that the RSE values for all components increased two to three-fold. Encouraging, however, was the notable difference in per unit area precision between instruments when measurement error was integrated. (Table 9). The relative proportions of SE due to measurement, model and sampling error using SRM were 11%, 66% and 23%, respectively. The relative proportions of SE due to measurement, model and sampling error using the TLS were 5%, 70% and 25%, respectively. Improvements in the measurement error from TLS were largely the result of increased accuracy of tree height as well as height to crown base. We acknowledge that the manual nature of the vegetation removal and the extraction of individual trees from co-registered scans possibly resulted in optimistic values of error contribution from the TLS. Nonetheless, our findings suggest using the TLS can result in a lower propagated error, primarily due to a smaller contribution to the total uncertainty from measurement error.

4. Conclusion

With broad-scale inventories, such as FIA and others likely to face an increased demand for defensible AGB uncertainty estimates, accounting for and addressing all primary sources of error becomes paramount. Taking the Monte Carlo approach shown here, measurement and model error have been successfully integrated and accounted for. With only 25 subjectively selected trees for use in comparison, the inference made here is an approximation. However, not only were the general contributions for all three sources of error illustrated, the addressal of measurement error was made by showing that the use of the TLS indeed can improve precision of per unit area estimation of lodgepole pine AGB using the component equations presented here.

Future research into this matter could also be best directed at similarly assessing the propagated error from using the TLS with other AGB models, as well as models for other parameters of interests, both point-in-time and growth-related. The TLS data analysis techniques shown here hold value in reducing uncertainty attributed to measurement error, which has been shown to contribute a potentially serious amount to the total per unit area uncertainty AGB estimates. Investigations into using the same multi-scan approach for plot-level analysis would add credence to the work done here, as that is likely the more applicable inventory scenario forest managers would be utilizing the TLS, rather than for single trees, as was done in this study. Extraction of additional tree-level input variables, such as upper stem diameters, merchantable top height and crown width would provide additional information about how the performance of the TLS in extracting these variables propagates up to per unit estimates of AGB. All of these future research efforts are likely to increase the defensibility of reported precision estimates for AGB derived using individual-tree equations, while also helping determine under which scanning scenarios, and for which input variables, does the use of the TLS translate into quantifiable gains in precision for broad-scale estimates of AGB.

Acknowledgments

We gratefully acknowledge the cooperation and support provided by several people in various phases of this project. Thanks are due to Andy Gray and James Westfall for their support and encouragement.

References

Avery, T. E., and Burkhart, H. E. (2002). Forest measurements (No. Ed. 5). McGraw- Hill Book Company.

Baskerville, G.L. 1972. Use of logarithmic regression in the estimation of plant biomass. Can. J. of For. Res. 2(1):49-53

Berger. A., Gschwantner, R.E., McRoberts, R.E., and Schadauer, K. 2014. Effects of measurement errors on individual tree stem volume estimates for the Austrian National Forest Inventory. For. Sci. 60(1):14-24

Bienert, A., Scheller, S., Keane, E., Mullooly, G., and Mohan, F. 2006. Application of terrestrial laser scanners for the determination of forest inventory parameters. International Archives of Photogrammetry, Remote Sensing and Spatial Information Sciences. 36(5).

Breidenbach, J., Antón-Fernández, C., Petersson H., Astrup, P., and McRoberts, R.E. 2014. Quantifying the model-related variability of biomass stock and change estimates in the Norwegian National Forest Inventory. For. Sci. 60(1):25-33

Calders, K., Newnham, G., Burt, A., Murphy, S., Raumonen, P., Herold, M., and Kaasalainen, M. (2015). Nondestructive estimates of above-ground biomass using terrestrial laser scanning. Methods in Ecology and Evolution, 6(2): 198-208.

Chasmer, L., Hopkinson, C., and Treitz, P. 2006. Investigating laser pulse penetration through a conifer canopy by integrating airborne and terrestrial lidar. Can. J. of Rem. Sens. 32(2):116-125.

Cunia, T. 1965. Some theory on reliability of volume estimates in a forest inventory sample. For. Sci., 11(1):115-128.

FARO. 2014. Techsheet of Laser Scanner FARO Focus^{3D} 120. http://www.faro.com

Hackenberg, J., Wassenberg, M., Spiecker, H., & Sun, D. 2015. Nondestructive method for biomass prediction combining TLS derived tree volume and wood density. Forests, 6(4), 1274-1300.

Henning, J. G., and Radtke, P. J. 2006. Detailed stem measurements of standing trees from ground-based scanning lidar. For. Sci. 52(1): 67-80.

Henning, J. G., and Radtke, P. J. 2006. Ground-based laser imaging for assessing three dimensional forest canopy structures. Photo. Eng. and Rem. Sens. 72(12): 1349.

Hopkinson, C., Chasmer, L., Young-Pow, C., and Treitz, P. 2004. Assessing forest metrics with a ground-based scanning lidar. Can. J. of For. Res. 34(3): 573-583.

Jung, S. E., Kwak, D. A., Park, T., Lee, W. K., and Yoo, S. 2011. Estimating crown variables of individual trees using airborne and terrestrial laser scanners. Rem. Sens. 3(11): 2346-2363.

Kim, S., McCaughey, R. J., Andersen, H. E., & Schreuder, G. 2009. Tree species differentiation using intensity data derived from leaf-on and leaf-off airborne laser scanner data. Rem. Sens. of Env., 113(8), 1575-1586.

Liang, X., V. Kankare, X. Yu, and J. Hyyppa, and M. Holopainen. 2014. Automated stem curve measurement using terrestrial laser scanning. IEEE transactions on geoscience and remote sensing. 52 (3): 1739-1748.

Maas, H. G., Bienert, A., Scheller, S., and Keane, E. 2008. Automatic forest inventory parameter determination from terrestrial laser scanner data. Int. J. of Rem. Sens. 29(5): 1579-1593.

Maisonobe, L. 2007. Finding the circle that best fits a set of points. October 25th.

MATLAB version 2013b. Natick, Massachusetts: The MathWorks Inc., 2013

McRoberts, R.E., and Westfall, J.A. 2014. Effects of uncertainty in model predictions of individual tree volume on large area volume estimates. For. Sci. 60(1):34-42

Pesonen, A., Maltamo, M., Eerikäinen, K., & Packalèn, P. 2008. Airborne laser scanning-based prediction of coarse woody debris volumes in a conservation area. Forest Ecology and Management, 255(8), 3288-3296.

Popescu, S. C., and Zhao, K. 2008. A voxel-based lidar method for estimating crown base height for deciduous and pine trees. Remote Sensing of Environment. 112(3):767-781.

Poudel, K.P. and H. Temesgen. 2016. Methods for estimating aboveground biomass and its components for Douglas-fir and lodgepole pine trees. Canadian Journal of Forest Research. 46: 77–87 (2016). dx.doi.org/10.1139/cjfr-2015-0256.

Poudel, K.P., H. Temesgen, and A.N. Gray. 2015. Evaluation of Sampling Strategies to Estimate Crown Biomass of Conifers. Forest Ecosystems, 2:1-11.

Pueschel, P., Newnham, G., Rock, G., Udelhoven, T., Werner, W., and Hill, J. 2013. The influence of scan mode and circle fitting on tree stem detection, stem diameter and volume extraction from terrestrial laser scans. ISPRS J. of Photo. and Rem. Sen. (77):44-56.

R Core Team 2012. R: A language and environment for statistical computing. R Foundation for Statistical Computing, Vienna, Austria. ISBN 3-900051-07-0, URL http://www.Rproject.org/

SAS Institute Inc. Output for this paper was generated using SAS software, Version 9.4 of the SAS System for Windows. Copyright © 2013 SAS Institute Inc. SAS and all other SAS Institute Inc. product or service names are registered trademarks or trademarks of SAS Institute Inc., Cary, NC, USA.

Shettles, M., Temesgen, H., Gray, A. N., & Hilker, T. 2015. Comparison of uncertainty in per unit area estimates of aboveground biomass for two selected model sets. Forest Ecology and Management, 354, 18-25.

Simonse, M., Aschoff, T., Spiecker, H., and Thies, M. 2003. Automatic determination of forest inventory parameters using terrestrial laser scanning. Proceedings of the ScandLaser Scientific Workshop on Airborne laser scanning of forests. 2003: 252-258.

Skovsgaard, J.P., Johannsen, V.K., and Vanclay, J.K. 1998. Accuracy and precision of two laser dendrometers. Forestry 71:131-139

Temesgen, H., D. Affleck, K.P. Poudel, A. Gray, and J. Sessions. 2015. A review of the challenges and opportunities in estimating above ground forest biomass using tree-level models. Scandinavian Journal of Forest Research. 30(4): 326-335

Temesgen, H., M.E. Goerndt, G. P. Johnson, D.M. Adams, and R.A. Monserud. 2007. Forest measurement and biometrics in forest management: status and future needs of the Pacific Northwest USA. Journal of Forestry. 105: 233-238

Thies M., Pfeifer, N., Winterhalder, D., and Gorte, B. G. 2004. Three-dimensional reconstruction of stems for assessment of taper, sweep and lean based on laser scanning of standing trees. Scand. J. of For. Res. 19(6): 571-581.

Vanclay, J.K., Skovsgaard, J.P. 1997. Evaluating forest growth models. Ecol. Model. 98(1):1-12

Weiß, J. 2009. Application and statistical analysis of terrestrial laser scanning and forest growth simulations to determine selected characteristics of Douglas-Fir stands. Folia For Pol. Ser A(51): 123-137.

Weiskittel, A. R., Hann, D. W., Kershaw Jr, J. A., and Vanclay, J. K. 2011. Forest growth and yield modeling. John Wiley & Sons.

Yu, X., Liang, X., Hyyppä, J., Kankare, V., Vastaranta, M., and Holopainen, M. 2013. Stem biomass estimation based on stem reconstruction from terrestrial laser scanning point clouds. Rem. Sens. Lett. 4(4): 344-353.

List of Tables

Table 1: TLS technical data

Specification	Focus^{3D} 120
Range Finder	Phase shift
Field of view (horizontal x vertical)	360° x 305°
Measurement range	0.6m – 120m
Distance accuracy	± 2mm at 25m
Sampling Rate	Up to 976k/sec
Beam radius at discharge	3.0mm
Beam divergence	0.19mrad (0.011°)
Weight	5.0kg

Table 2: Summary statistics of the measurements errors for STM and TLS

	Standing Tree Measurements (STM)				
	n	**Min.**	**Mean**	**Max.**	**SD**
HT (m)	25	-2.56	-0.98	0.12	0.67
HTCB (m)	25	-1.04	-0.06	1.37	0.52
	Terrestrial LiDAR (TLS)				
	n	**Min.**	**Mean**	**Max.**	**SD**
DBH (cm)	25	-1.27	-0.25	1.52	0.51
HT (m)	25	-0.79	-0.06	0.55	0.27
HTCB (m)	25	-3.29	0.49	3.90	1.68

Table 3: Model predictions and RMSE values for CRM ratios and CRM tree-level estimates without measurement error. Tree-levels units are in kilograms of dry biomass.

Model Means-Without Measurement Error			**Model RMSEs-Without Measurement Error**		
Total Tree (SUR)	287.11		**Total Tree (SUR)**	70.59	
Component	**CRM Ratios**	**CRM Tree-Level**	**Component**	**CRM Ratios**	**CRM Tree-Level**
Bole	0.672	193.07	**Bole**	0.067	51.24
Bark	0.055	15.66	**Bark**	0.034	10.62
Branch	0.195	56.04	**Branch**	0.055	21.02
Foliage	0.082	23.40	**Foliage**	0.022	8.63

Table 4: Model predictions for CRM ratios and CRM tree-level estimates with measurement error, for STM and TLS. Tree-levels units are in kilograms of dry biomass.

Model Means-With Measurement Error				
Total Tree (SUR)-STM	287.11			
Total Tree (SUR)-TLS	296.57			
	STM	**TLS**	**STM**	**TLS**
Component	**CRM Ratios**	**CRM Ratios**	**CRM Tree-Level**	**CRM Tree-Level**
Bole	0.599	0.620	172.03	177.97
Bark	0.061	0.061	17.45	17.47
Branch	0.209	0.208	60.11	59.80
Foliage	0.091	0.091	26.19	26.21

Table 5: Model RMSE values for CRM ratios and CRM tree-level estimates with measurement error, for STM and TLS. Tree-levels units are in kilograms of dry biomass.

Model RMSEs-With Measurement Error				
Total Tree (SUR)-STM	70.59			
Total Tree (SUR)-TLS	174.70			
	STM	**TLS**	**STM**	**TLS**
Component	**CRM Ratios**	**CRM Ratios**	**CRM Tree-Level**	**CRM Tree-Level**
Bole	0.297	0.067	95.30	123.09
Bark	0.047	0.034	14.04	15.16
Branch	0.074	0.055	25.81	43.16
Foliage	0.037	0.022	12.46	19.19

683 Table 6: Per hectare estimates and SE values for CRM equations, without accounting for measurement or model error. Units are in kilograms of dry biomass
684 per hectare.

Sampling Error Only		
Component	**Mean**	**SE**
Bole	23,270.38	4,945.90
Bark	1,842.11	357.83
Branch	6,414.97	1,234.54
Foliage	2,544.31	463.86

Table 7: Per hectare estimates and SE values for CRM equations accounting for model error. Units are in dry kilograms of biomass per hectare.

Sampling Error (With Model Error)		
Component	**Mean**	**SE**
Bole	37,062.80	17,659.36
Bark	4,947.56	3,317.42
Branch	9,275.29	4,043.61
Foliage	3,425.94	1,234.22

Table 8: Per hectare estimates and SE values for CRM equations accounting for model error. Units are in dry kilograms of biomass per hectare.

Sampling Error (With Model and Measurement Error)					
Mean			**SE**		
Component	**STM**	**TLS**	**Component**	**STM**	**TLS**
Bole	37,819.12	37,442.94	**Bole**	19,201.47	18,583.77
Bark	3,984.19	3,740.49	**Bark**	4,502.45	3,429.02
Branch	9,475.49	9,475.52	**Branch**	4,266.80	4,363.27
Foliage	3,512.56	3,547.24	**Foliage**	1,316.67	1,355.31

Table 9: RSE values for CRM equations accounting for model and measurement error.

Sampling Error (RSEs)				
	Sampling Only	**Model Errors**	**Model and Measurement Errors**	
Component			**STM**	**TLS**
Bole	21.3%	47.6%	50.8%	49.6%
Bark	19.4%	67.1%	113.0%	91.7%
Branch	19.2%	43.6%	45.0%	46.0%
Foliage	18.2%	36.0%	37.5%	38.2%

List of Figures

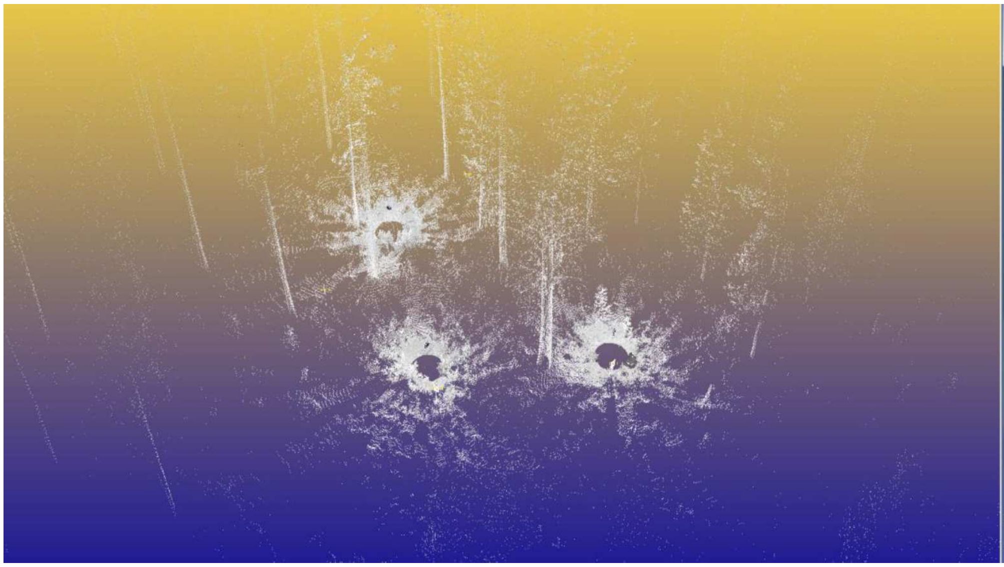

Filtered overhead 3D view of registered point cloud. Black circles denote scan locations around the sample tree, located right center.
839x469mm (72 x 72 DPI)

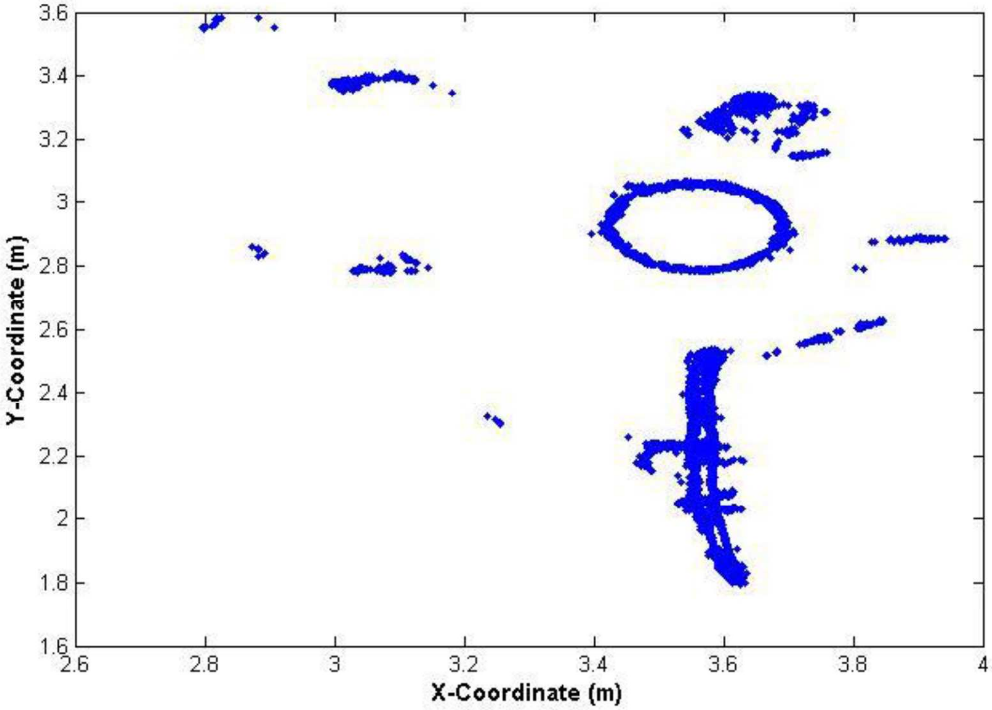

Birds eye view of detection slice taken at 1.37m above the lowest point in the point cloud. Unrestricted subset included branches and foliage located within the height range of the slice.
769x552mm (72 x 72 DPI)

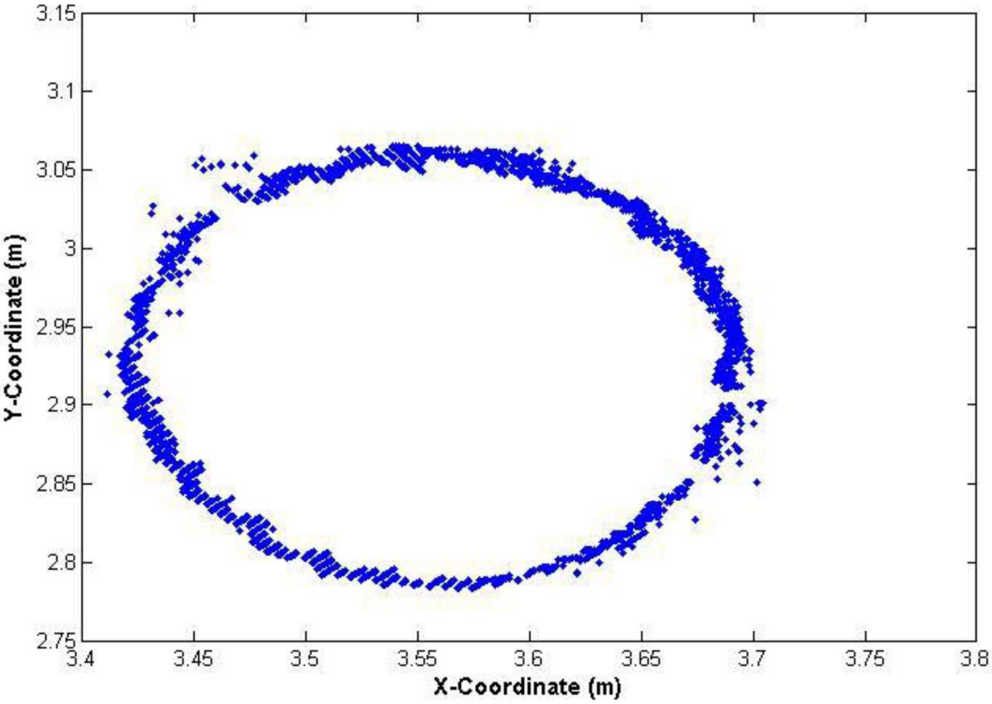

Birds eye view of detection slice taken at 1.37m above the lowest point in the point cloud. Unrestricted subset included branches and foliage located within the height range of the slice.
778x542mm (72 x 72 DPI)

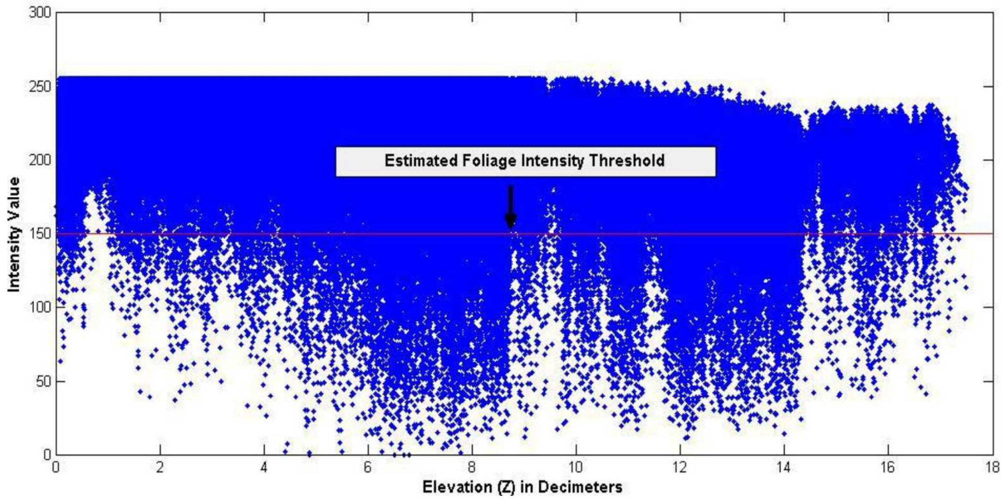

Graph of intensity values versus elevation for 0.1m height bins. Subjectively determined subset threshold is shown in red.
744x371mm (72 x 72 DPI)